Published in final edited form as:
J Neurosci Methods. 2014 April 30; 227: 159–165. doi:10.1016/j.jneumeth.2014.02.005.

Morphological analysis of neuromuscular junction development and degeneration in rodent lumbrical muscles

James N. Sleigh[1,2], **Robert W. Burgess**[3], **Thomas H. Gillingwater**[4], and **M. Zameel Cader**[1,2,*]

[1]Nuffield Department of Clinical Neurosciences, University of Oxford, John Radcliffe Hospital, Oxford OX3 9DU, UK

[2]The Weatherall Institute of Molecular Medicine, University of Oxford, John Radcliffe Hospital, Oxford OX3 9DS, UK

[3]The Jackson Laboratory, Bar Harbor, ME 04609, USA

[4]Centre for Integrative Physiology & Euan MacDonald Centre for Motor Neurone Disease Research, University of Edinburgh, Edinburgh EH8 9XD, UK

Abstract

Background—The neuromuscular junction (NMJ) is a specialised synapse formed between a lower motor neuron and a skeletal muscle fibre, and is an early pathological target in numerous nervous system disorders, including amyotrophic lateral sclerosis (ALS), Charcot-Marie-Tooth disease (CMT), and spinal muscular atrophy (SMA). Being able to accurately visualize and quantitatively characterise the NMJ in rodent models of neurological conditions, particularly during the early stages of disease, is thus of clear importance.

New Method—We present a method for dissection of rodent deep lumbrical muscles located in the hind-paw, and describe how to perform immunofluorescent morphological analysis of their NMJs.

Results—These techniques allow the temporal assessment of a number of developmental and pathological NMJ phenotypes in lumbrical muscles.

Comparison with Existing Methods—Small muscles, such as the distal hind-limb lumbrical muscles, possess a major advantage over larger muscles, such as *gastrocnemius*, in that they can be whole-mounted and the entire innervation pattern visualised. This reduces preparation time and ambiguity when evaluating important neuromuscular phenotypes.

*Corresponding author: Dr. M Zameel Cader Nuffield Department of Clinical Neurosciences, University of Oxford, John Radcliffe Hospital, Oxford OX3 9DU, UK. Tel: +44 (0)1865 231893 Fax: +44 (0)1865 231885 zameel.cader@ndcn.ox.ac.uk.

Conflict of Interest Statement. None declared.

Conclusions—Together, these methods will allow the reader to perform a detailed and accurate analysis of the neuromuscular system in rodent models of disease in order to identify pertinent features of neuropathology.

Keywords

lower motor neuron; lumbrical muscle; neurodegeneration; neurodevelopment; neuromuscular disease; neuromuscular junction (NMJ)

1. Introduction

The mammalian neuromuscular junction (NMJ) is a peripheral synapse that functionally couples lower motor neurons to skeletal muscle fibres. Formed during pre-natal development, the highly specialised NMJ efficiently transfers information from a pre-synaptic motor nerve to a post-synaptic muscle fibre, permitting rapid muscle contraction in response to neuronal stimulation. Due to its relatively large size, experimental tractability, and simplicity, the NMJ has been used as a model for many years to better understand the general principals of synaptic establishment, structure, development, and function (Sanes and Lichtman, 1999).

Pathological targeting of the NMJ is a characteristic feature of a number of neurological conditions, including amyotrophic lateral sclerosis (Fischer et al., 2004; Tsujihata et al., 1984), Charcot-Marie-Tooth diseases (d'Ydewalle et al., 2011; Sleigh et al., 2014), and spinal muscular atrophy (Martínez-Hernández et al., 2012; Murray et al., 2008a). The NMJ is also the primary target in myasthenic disorders such as myasthenia gravis (Spillane et al., 2010), and serves as an entry-point for a number of potent neurotoxins (Caleo and Schiavo, 2009). Furthermore, degeneration of the NMJ precedes axon loss in response to axotomy (Gillingwater and Ribchester, 2001), and is a hallmark of aging (Valdez et al., 2010; Wokke et al., 1990). It is therefore of paramount importance to be able to accurately image and quantify connectivity between lower motor nerves and muscle fibres at the NMJ.

Much of what is known about the mammalian NMJ has been gleaned from experiments in mice and rats, as they provide a ready source of tissue for imaging NMJs using immunofluorescence and electron microscopy. The availability of transgenic mice expressing fluorescent proteins in select cells/tissues (e.g. nerves or muscles) (Lichtman and Sanes, 2003), in combination with a wealth of disease models (Burgess et al., 2010; Sleigh et al., 2011; Turner and Talbot, 2008), has undoubtedly facilitated this understanding of the synapse in both health and disease. Large muscles of the rodent hind-limb, such as *gastrocnemius* or *tibialis anterior*, have typically been used to examine NMJs using immunofluorescent labelling. However, to obtain levels of antibody penetration required for efficient NMJ visualisation, these muscles require sectioning, which increases sample preparation time and can lead to ambiguity when evaluating certain neuromuscular phenotypes through sectioning artefacts, inconsistent fixation, and challenges in imaging associated with thick samples. Smaller muscles that can be dissected and whole-mounted possess the major advantage that the entire innervation pattern can be observed without sectioning, permitting a more precise assessment of NMJ development, degeneration, and

regeneration (Murray et al., 2010a). For instance, selectively vulnerable populations of synapses and nodal sprouting in response to injury can only be accurately studied in intact whole muscles (Murray et al., 2012; Murray et al., 2008a).

The deep lumbrical muscles of the rodent hind-limb are located between the digits. Originating from the ventral surface of the *flexor digitorum longus* (FDL) tendon, the lumbricals aid metatarsophalangeal joint flexion and are thus required for paw clasping. These muscles consist of predominantly fast-twitch muscle fibres, and are innervated by terminal branches of the tibial nerve (Betz et al., 1980a, b). The lumbricals are small (1–2 mm long), relatively thin (<500 μm), and possess between •70–230 myofibres (all numbers pertain to young adult mice) (Clark et al., 1987), so can be dissected and the entire neuromuscular architecture visualised in whole-mount preparations using fluorescence microscopy (Costanzo et al., 1999; Murray et al., 2008a; Murray et al., 2008b; Sleigh et al., 2014), making them ideal for connectome analysis similar to that performed in the interscutularis muscle (Lu et al., 2009). Rodent lumbrical muscles have also been used in pharmacological and electrophysiological experiments, as well as morphological studies using electron and Nomarski microscopy (Clark et al., 1987; Dieler et al., 1992; Jirmanova, 1975).

Here, we describe a simple, modified technique for dissecting the first to fourth deep lumbricals of mouse and rat hind-limbs, in order to visualise the entire innervation pattern. In addition, we outline the immunofluorescence staining protocol and how to generate clear confocal images of NMJs. Finally, we discuss how to assess various developmental and degenerative phenotypes of the synapse, which can be applied to any muscle, in order to perform a detailed analysis of the rodent neuromuscular system through time.

2. Materials and Methods

2.1 Reagents

The following reagents are required: AlexaFluor 488 secondary antibody (goat anti-mouse, Invitrogen A-11001), anti-2H3 (supernatant, IgG1, mouse, DSHB), anti-SV2 (concentrate, IgG1, mouse, DSHB), bovine serum albumin (BSA, Sigma B4287), 1,4-diazabicyclo[2.2.2]octane (DABCO, Sigma D27802), distilled water, glycerol (Sigma G5516), Mowiol 4–88 (Calbiochem 475904), 16% paraformaldehyde (PFA, Electron Microscopy Sciences 15710), 10X phosphate buffered saline (PBS, 1.37 M NaCl [Sigma S3014], 100 mM Na_2HPO_4 [Sigma S3264], 27 mM KCl [Sigma P9541], 20 mM KH_2PO_4 [Sigma P9791]), Sylguard 184 silicone elastomer kit (Dow Corning 01015311), tetramethylrhodamine -bungarotoxin (-BTX, Cambridge Bioscience BT00012), Triton X-100 (Sigma T8787), and Trizma hydrochloride (Sigma T5941).

2.2 Equipment and Software

The following pieces of equipment, or similar alternatives, are required: bone scissors (Fine Science Tools 14110-15), 22 × 22 mm coverslips (Fisher Scientific 12333128), 50 ml conical flask (Corning 70980), 1.5 ml Eppendorf tubes (Eppendorf 3810X) forceps (Fine Science Tools 11251-10), 15 and 50 ml Falcon tubes (BD Falcon 352097 and 352070), LSM

510 META laser scanning microscope (Zeiss), magnetic stirrer and stir bar (VWR 442-0883 and 442-0272), 25 × 75 mm microscope slides (Fisher Scientific 10149870), 12 × 0.2 mm minutiens insect pins (Austerlitz 0.20), 60 × 15 mm petri dishes (BD Biosciences 351007), 3 ml plastic Pasteur pipette (Appleton Woods KS230), rocker (VWR 444-0116), spring scissors (Fine Science Tools 15000-08), SZB 250 dissection microscope (VWR 630-1577), water bath (VWR 462-0242), and 24- and 96-well tissue culture plates (BD Falcon 353047 and 353075). ImageJ (http://rsb.info.nih.gov/ij/) was used for projecting Z-stack images, and measuring NMJ area and average endplate fluorescence intensity. Figures were compiled using GraphPad Prism 5 and Adobe Photoshop CS5 software.

2.3 Reagent Setup

Mowiol mounting medium was made by adding 2.4 g of Mowiol 4–88 and 6 g of glycerol to 12 ml distilled water in a 50 ml conical flask and mixing overnight on a magnetic stirrer. The following day, 12 ml of 0.2 M Trizma hydrochloride (pH 8.5) was added, and the medium heated in a water bath at 55°C for 2 h with regular mixing. Finally, 0.72 g of DABCO (w/v) was added. The medium was aliquoted into Eppendorf tubes to avoid repeated freeze-thaw cycles, and stored at −20°C for up to a year. 10X PBS was stored at room temperature (18–22°C) and diluted in distilled water to a 1X working solution, which was used within a month. 16% PFA was diluted in distilled water to a 4% working solution, and used on the day of preparation. Permeabilisation, blocking, and antibody solutions were all used on the day of preparation. Sylguard 184 silicone elastomer was prepared by combining the elastomer base to the curing agent in a 10:1 ratio, pouring into petri dishes, and allowing to set for at least 48 h.

2.4 Animals

Animal handling and experiments performed in the UK conformed to the Home Office Animals (Scientific Procedures) Act (1986) and were approved by the University of Oxford Ethical Review Panel, while those completed in the US were conducted in accordance with the NIH Guide for Care and Use of Laboratory Animals and approved by The Jackson Laboratory Animal Care and Use Committee. $Gars^{Nmf249/+}$ mice were maintained as heterozygote breeding pairs on a predominantly C57BL/6 background as previously described (Seburn et al., 2006; Stum et al., 2010).

2.5 Dissection of hind-limb lumbrical muscles

The first to fourth deep lumbrical muscles were dissected from the left hind-leg of post-natal day 15 (P15) and two month-old mice (Fig. 1). Animals were culled via cervical dislocation before detaching the hind-legs using bone scissors. The overlying skin was removed by cutting along the dorsal midline in a proximal to distal fashion to the base of the foot. The foot was pinned down ventral side up in a Sylguard 184 silicone elastomer-covered petri dish using insect pins and immersed in chilled 1X PBS. A dissection microscope was used for all subsequent steps. The remaining plantar skin covering the central region of the foot was removed revealing the underlying plantar hypodermal surface (Fig. 1A). Before reaching the FDL tendon, where the lumbricals originate, the overlying *flexor digitorum brevis* (FDB) tendon was removed. This was done by making a transverse cut near to the

ankle, peeling the FDB tendon distally towards the toes, and then severing the distal parts of the tendon at the metatarsophalangeal joint. Once removed, a similar process was repeated for the FDL tendon (Fig. 1B), but this time also cutting the tissues distal to the lumbricals (Fig. 1C) freeing the entire plantar muscle mass (Fig. 1D). The FDL tendon was pinned out tautly in the dish ventral side up (Fig. 1E). Surrounding connective tissue was then carefully blunt dissected away to reveal the underlying lumbrical muscles between the distal ends of the tendon (Fig. 1F and G). Muscles were fixed for 10 min in freshly prepared PBS containing 4% (w/v) PFA. This stage should be completed within an hour of starting the dissection in order to reduce tissue decay. This method is not suited to PFA-perfused animals, as the prolonged fixation process hinders the dissection and results in sub-optimal antibody binding. Once fixed and washed with 1X PBS, further connective tissue was detached from the muscles, and individual fibres were carefully teased apart to facilitate antibody penetration. The lumbricals were then separated from the FDL tendon (Fig. 1H), pinned out, and further cleared of unwanted tissue. Finally, the remaining distal part of the FDB tendon was removed before starting the staining protocol (Fig. 1I).

2.6 Muscle immunohistochemistry and NMJ imaging

Muscles were permeabilised in 24/96-well plates with 2% (v/v) Triton X-100 in PBS for 30 min. They were blocked in 4% (w/v) BSA and 1% (v/v) Triton X-100 in PBS for 30 min. Samples were incubated overnight at 4°C in blocking solution with primary antibodies against neurofilament (2H3, 1/50) and synaptic vesicles (SV2, 1/100) in order to visualise the axons and pre-synaptic nerve terminals, respectively. A synaptophysin antibody (1/200, IgG1, mouse, Milipore MAB368) can be used in place of anti-SV2 (Cobb et al., 2013). The following day, muscles were washed three times for 30 min in PBS before incubation for 2 h with AlexaFluor 488 secondary antibody (1/250) and 1.5 μg/ml tetramethylrhodamine -BTX in PBS. From this point onwards, care was taken to protect the samples from light. Finally, muscles were washed three times for 30 min in PBS, and mounted in Mowiol on microscope slides with coverslips. Since the lumbricals are <500 μm thick, there is no need to adjust for muscle thickness when mounting. Slides were left at 4°C overnight to allow the Mowiol to set before imaging. All incubation and wash steps were performed on a rocker, and at room temperature unless otherwise stated. Muscles were carefully transferred using forceps to new wells when incubating and washing. A Zeiss LSM 510 META laser scanning microscope equipped with 30 mW Argon and HeNe 543 nm lasers was used to image the neuromuscular system, which was labelled green for nervous tissue (2H3 and SV2) and red for post-synaptic acetylcholine receptors (AChRs, -BTX) (Fig. 2 and 3). A 63x/1.4NA Plan-Apo oil immersion objective was used to determine synapse elimination, plaque-to-pretzel transition and denervation, a 20x/0.75NA Plan-Apo oil objective was used to measure NMJ area and average -BTX fluorescence intensity, and a 10x/0.3NA Plan-Fluor air objective was used to produce the image in Fig. 2A. Sequential capture was used to separate the green and red channels in order to prevent crosstalk between dyes, and Z-stacks with 300 nm intervals were taken. Z-stacks were projected into single images using ImageJ (Image>Stacks>Z Project>Max Intensity) and the resulting “collapsed” images used for all analyses. Only NMJs with clearly visible pre-synaptic axons and terminals should be scored, and ideally 40 or more NMJs should be assessed.

2.6.1 Synapse elimination—The process of synapse elimination at the NMJ is measured by calculating the percentage of polyinnervated endplates. Singly innervated NMJs possess one axonal input and have successfully undergone synapse elimination, whereas polyinnervated NMJs display more than one axonal input per endplate because extraneous branches have yet to retract (Fig. 3A) (Sanes and Lichtman, 1999). NMJs are only scored as polyinnervated when it is clear that two or more collateral inputs arise from separate axons and not from a single axon that has split before it reached the target endplate. A distance equal to at least the length of the endplate back from where the nerve reaches the post-synaptic staining should be assessed. An increased percentage of polyinnervated NMJs is indicative of delayed/defective synapse elimination.

2.6.2 Endplate morphological maturation—To measure the “plaque-to-pretzel” transition of the motor endplate (Marques et al., 2000), which is an indicator of post-synaptic maturation, the number of perforations per endplate can be counted (Fig. 3A). A perforation, or hole, is defined as a region in which there is no observable -BTX staining (labeling AChRs) within the circumference of the endplate. When scoring endplate maturation in animals less than two weeks of age, NMJs can be categorised as “plaques” with uniform AChR staining, “folded” with regions of brighter fluorescence, or “perforated”, as perforations have often not yet formed at these time-points (Misgeld et al., 2002; Murray et al., 2010b). NMJs not positioned perpendicular to the imaging plane (*en face*) should not be scored as perforations may be obscured.

2.6.3 NMJ growth and endplate fluorescence intensity—Measurement of NMJ area and average -BTX fluorescence intensity is performed on Z-stacks images in the red channel. Using ImageJ, the perimeter circumscribing the post-synaptic staining can be drawn by hand and the enclosed surface area (including the perforated area) and average intensity measured (Fig. 3B) (Bogdanik et al., 2013). First, the green and red channels must be separated (Image>Colour>Split Channels) and Z-stacks of the red channel projected into a single image. The “Freehand Selections” tool can then be used to draw around the perimeter of the endplate, allowing the contained area and average fluorescence intensity to be measured. The area in pixels can be converted into μm^2 based on the magnification and scale settings of the confocal microscope. Mean fluorescence intensity is expressed in arbitrary units. Once again, only *en face* NMJs should be scored. For comparison of fluorescence intensity it is essential that samples be processed in parallel and all images acquired using the same confocal settings (e.g. laser power, gain, magnification, image resolution, Z-stack total size, and Z-stack interval).

2.6.4 Denervation—Neuromuscular synapses can be scored for degenerative phenotypes by assessing the overlap between pre-synaptic SV2/synaptophysin and post-synaptic AChR staining, also termed NMJ ocupancy (Fig. 3C). NMJs with closely juxtaposed pre- and post-synaptic staining throughout are classified as being “fully innervated” (Fig. 2B), synapses with some endplate regions devoid of neuronal input are described as “partially denervated” (Fig. 3A), while NMJs with no pre-synaptic staining due to axonal loss are counted as “vacant” or “fully denervated” (Fig. 3C) (Comley et al., 2011). To increase accuracy, NMJs should be scored as partially denervated using an arbitrary cutoff value, for example when

•15 to <100% of the total endplate area lacks neuronal input. Alternatively, the percentage overlap in staining between the pre- and post-synapse can be assessed using confocal microscopy and ImageJ as outlined above (Dachs et al., 2011); however, care should be taken in the interpretation as pathological neurofilament accumulation may affect this readout.

3. Results and Discussion

We have developed a method to quickly dissect, and immunohistochemically label NMJs in mouse and rat hind-limb lumbrical muscles post-mortem without the need for specialist equipment (Fig. 1). With practice, these dissections can be successfully completed in 10–20 min per mouse and slightly longer in rats, allowing whole litters to be used within 2–4 h. The resulting lumbrical preparations are thin enough to be whole-mounted, obviating the need for sectioning and allowing the visualisation of the entire innervation pattern using epifluorescence or confocal microscopy (Fig. 2A). Using the described immunofluorescence staining protocol, clear low- and high-magnification micrographs of NMJs can be produced (Fig. 2), allowing the accurate analysis of numerous developmental and degenerative phenotypes pertinent to neuromuscular pathology (Fig. 3).

Assessment of NMJ Development

At birth the mammalian NMJ displays a number of key morphological features that undergo significant remodelling as the synapse develops in the early postnatal period (Sanes and Lichtman, 1999). We describe here how to quantitatively measure a number of these phenotypes in immunohistochemically-labelled rodent lumbrical muscle preparations, which has previously proven useful for identifying pathologies pertinent to mouse models of neuromuscular disorders (Murray et al., 2008a; Sleigh et al., 2014).

Synapse elimination is the process whereby supernumerary axonal inputs to polyneuronally-innervated endplates retract resulting in motor endplates innervated by only a single motor axon (Fig. 3A). This process is usually complete by two weeks in wild-type mice (Balice-Gordon and Lichtman, 1993; Walsh and Lichtman, 2003). It is determined by relative synaptic activity in the competing terminals and is thought to serve as a post-natal mechanism for refining neuronal architecture in response to the external environment (Buffelli et al., 2003; Sanes and Lichtman, 2001). NMJs can be scored as being singly innervated or polyinnervated by viewing the muscle preparations down a fluorescence microscope or by taking Z-stack images using a confocal microscope and scoring at a later time. Calculating the percentage of polyinnervated synapses allows for a simple assessment of the elimination process, and provides an easy way to measure pre-synaptic development.

Mirroring maturation of the motor neuron, the post-synaptic endplate transitions from a relatively simple, circular, plaque-like shape to a complex, pretzel-like structure. This occurs as AChRs increase in number and migrate to closely appose the pre-synaptic nerve terminal, allowing efficient acetylcholine release and receptor-binding. During this “plaque-to-pretzel” development (Marques et al., 2000), perforations in the post-synaptic -BTX staining can be observed where AChRs no longer reside. During the first post-natal week, wild-type mouse lumbrical motor endplates display very few, if any, post-synaptic perforations. By

two weeks, however, endplates usually possess two or more perforations, and by one month often more than five (Sleigh et al., 2014). Imaged in the same manner as synapse elimination, quantification of the number of perforations per NMJ serves as a measure for post-synaptic maturation and allows for comparison with pre-synaptic development. It is important to assess both phenotypes as pre- and post-synaptic pathologies do not necessarily correlate (Murray et al., 2008a).

To complete developmental phenotyping, we outline how to measure NMJ area and AChR staining intensity (Fig. 3C). These two features of the synapse increase over time due to organism growth and increased muscle fibre diameter, and have been shown to diverge from wild-type in mouse models of neurological disease (Bogdanik and Burgess, 2011; Bogdanik et al., 2012).

Assessment of NMJ Denervation

Lower motor neuron degeneration is a characteristic feature of a number of neuromuscular disorders, and the NMJ appears to be an early target for this pathological process in rodent disease models (Fischer et al., 2004; Murray et al., 2008a; Murray et al., 2010c; Sleigh et al., 2014). It is therefore important to be able to accurately determine levels of denervation at the neuromuscular synapse. Fully denervated synapses are easily identified because there is no neuronal staining overlying the -BTX staining (Fig. 3C). However, deciding whether a NMJ is fully innervated (Fig. 2B) or partially denervated (Fig. 3A) is a little more subjective; a pre-determined numerical cut-off for the percentage of the post-synapse lacking input should therefore be used. Care should also be taken to ensure that the lack of pre-synaptic staining is not simply due to poor antibody penetration. This can be determined by observing the surrounding NMJs; if all of the neighbouring synapses lack neuronal staining, but display endplates with crisp exteriors and complex pretzel conformations, it is likely that the staining protocol has failed to label the entire nervous. A secondary indicator of denervation is diffuse and/or reduced intensity of endplate staining, which is caused by the lack of neuronal signal and subsequent AChR dispersal (Fig. 3A).

Conclusion

Rodent hind-limb lumbrical muscles can be quickly dissected and, due to their small size and thin nature, the entire innervation pattern visualised using immunofluorescence microscopy. This allows for the accurate assessment of developmental and degenerative neuromuscular phenotypes, including those outlined here and others - for example, terminal and nodal sprouting (Murray et al., 2010b), paralysis-induced remodeling (Murray et al., 2008a), neurofilament accumulation/axonal swelling (Ling et al., 2012; Valdez et al., 2010), terminal Schwann cell number, morphology, and sprouting (Murray et al., 2012), active zone density (Chen et al., 2012), active zone association with synaptic vesicles (Torres-Benito et al., 2011), mitochondrial density and microtubule maturity (Torres-Benito et al., 2011), intramuscular axon numbers (Murray et al., 2010b), and AChR subunit-switching (Kong et al., 2009). We have used a mouse model of the peripheral neuropathy Charcot-Marie-Tooth disease type 2D (*Gars*$^{Nmf249/+}$) to demonstrate the utility of the lumbrical muscle preparation for highlighting pathological NMJ phenotypes. Many of these

phenotypes are also seen in wild-type mice older than one year (Valdez et al., 2010), suggesting that the presence of these defects in younger animals is an early indicator of a malfunctioning neuromuscular system. Different muscles are known to show differential susceptibility to disease (Santos and Caroni, 2003; Thomson et al., 2012; Valdez et al., 2010); lumbrical muscle NMJs should therefore be compared with similar whole-mount preparations, such as the diaphragm (Wu and Mei, 2013), the cranial muscles (Lu et al., 2009; Murray et al., 2010a), the *transversus abdominis* (Murray et al., 2014), and the *triangularis sterni* (McArdle et al., 1981). In combination, the methods presented here provide an accurate way to discern pertinent features of neuromuscular pathology often observed in rodent models of nervous system disease.

Acknowledgments

The authors would like to thank Kevin L. Seburn, Eilidh Somers, and Sophie R. Thomson for experimental advice and helpful discussions. JNS is also grateful for the support of Somerville College, Oxford and a Fulford Junior Research Fellowship. Work in Dr. M. Zameel Cader's laboratory is supported by grants from the Oxford Biomedical Research Centre and the French Muscular Dystrophy Association (AFM). Professor Thomas H. Gillingwater receives research funding from the Muscular Dystrophy Campaign and the SMA Trust. Dr. Robert W. Burgess is funded by the National Institutes of Health [NS054154, NS079677]. The 2H3 and SV2 antibodies (developed by Thomas M. Jessell/Jane Dodd and Kathleen M. Buckley, respectively) were obtained from the Developmental Studies Hybridoma Bank maintained by The University of Iowa, Department of Biology. The funders had no role in study design, data collection and analysis, decision to publish, or preparation of the manuscript.

All authors have read and approved submission of this work.

Abbreviatons

-BTX	-bungarotoxin
AChR	acetylcholine receptor
BSA	bovine serum albumin
DABCO	1,4-diazabicyclo[2.2.2]octane
FDB	flexor digitorum brevis
FDL	flexor digitorum longus
NMJ	neuromuscular junction
PFA	paraformaldehyde

6. References

Balice-Gordon RJ, Lichtman JW. *In vivo* observations of pre- and postsynaptic changes during the transition from multiple to single innervation at developing neuromuscular junctions. J Neurosci. 1993; 13:834–55. [PubMed: 8426240]

Betz WJ, Caldwell JH, Ribchester RR. The effects of partial denervation at birth on the development of muscle fibres and motor units in rat lumbrical muscle. J Physiol. 1980a; 303:265–79. [PubMed: 7431234]

Betz WJ, Caldwell JH. Ribchester RR. Sprouting of active nerve terminals in partially inactive muscles of the rat. J Physiol. 1980b; 303:281–97. [PubMed: 7431235]

Bogdanik LP, Burgess RW. A valid mouse model of AGRIN-associated congenital myasthenic syndrome. Hum Mol Genet. 2011; 20:4617–33. [PubMed: 21890498]

Bogdanik LP, Chapman HD, Miers KE, Serreze DV, Burgess RW. A MusD retrotransposon insertion in the mouse *Slc6a5* gene causes alterations in neuromuscular junction maturation and behavioral phenotypes. PLoS One. 2012; 7:e30217. [PubMed: 22272310]

Bogdanik LP, Sleigh JN, Tian C, Samuels ME, Bedard K, Seburn KL, Burgess RW. Loss of the E3 ubiquitin ligase LRSAM1 sensitizes peripheral axons to degeneration in a mouse model of Charcot-Marie-Tooth disease. Dis Model Mech. 2013; 6:780–92. [PubMed: 23519028]

Buffelli M, Burgess RW, Feng G, Lobe CG, Lichtman JW, Sanes JR. Genetic evidence that relative synaptic efficacy biases the outcome of synaptic competition. Nature. 2003; 424:430–4. [PubMed: 12879071]

Burgess RW, Cox GA, Seburn KL. Neuromuscular disease models and analysis. Methods Mol Biol. 2010; 602:347–93. [PubMed: 20012408]

Caleo M, Schiavo G. Central effects of tetanus and botulinum neurotoxins. Toxicon. 2009; 54:593–9. [PubMed: 19264088]

Chen J, Mizushige T, Nishimune H. Active zone density is conserved during synaptic growth but impaired in aged mice. J Comp Neurol. 2012; 520:434–52. [PubMed: 21935939]

Clark AW, Bandyopadhyay S, DasGupta BR. The plantar nerves-lumbrical muscles: a useful nerve-muscle preparation for assaying the effects of botulinum neurotoxin. J Neurosci Methods. 1987; 19:285–95. [PubMed: 3586701]

Cobb MS, Rose FF, Rindt H, Glascock JJ, Shababi M, Miller MR, Osman EY, Yen PF, Garcia ML, Martin BR, Wetz MJ, Mazzasette C, Feng Z, Ko CP, Lorson CL. Development and characterization of an *SMN2*-based intermediate mouse model of Spinal Muscular Atrophy. Hum Mol Genet. 2013; 22:1843–55. [PubMed: 23390132]

Comley LH, Fuller HR, Wishart TM, Mutsaers CA, Thomson D, Wright AK, Ribchester RR, Morris GE, Parson SH, Horsburgh K, Gillingwater TH. ApoE isoform-specific regulation of regeneration in the peripheral nervous system. Hum Mol Genet. 2011; 20:2406–21. [PubMed: 21478199]

Costanzo EM, Barry JA, Ribchester RR. Co-regulation of synaptic efficacy at stable polyneuronally innervated neuromuscular junctions in reinnervated rat muscle. J Physiol. 1999; 521(Pt 2):365–74. [PubMed: 10581308]

d'Ydewalle C, Krishnan J, Chiheb DM, Van Damme P, Irobi J, Kozikowski AP, Vanden Berghe P, Timmerman V, Robberecht W, Van Den Bosch L. HDAC6 inhibitors reverse axonal loss in a mouse model of mutant HSPB1-induced Charcot-Marie-Tooth disease. Nat Med. 2011; 17:968–74. [PubMed: 21785432]

Dachs E, Hereu M, Piedrafita L, Casanovas A, Caldero J, Esquerda JE. Defective neuromuscular junction organization and postnatal myogenesis in mice with severe spinal muscular atrophy. J Neuropathol Exp Neurol. 2011; 70:444–61. [PubMed: 21572339]

Dieler R, Volker A, Schroder JM. Scanning electron microscopic study of denervated and reinnervated intrafusal muscle fibers in rats. Muscle Nerve. 1992; 15:433–41. [PubMed: 1533012]

Fischer LR, Culver DG, Tennant P, Davis AA, Wang M, Castellano-Sanchez A, Khan J, Polak MA, Glass JD. Amyotrophic lateral sclerosis is a distal axonopathy: evidence in mice and man. Exp Neurol. 2004; 185:232–40. [PubMed: 14736504]

Gillingwater TH, Ribchester RR. Compartmental neurodegeneration and synaptic plasticity in the Wld^S mutant mouse. J Physiol. 2001; 534:627–39. [PubMed: 11483696]

Jirmanova I. Ultrastructure of motor end-plates during pharmacologically-induced degeneration and subsequent regeneration of skeletal muscle. J Neurocytol. 1975; 4:141–55. [PubMed: 1123653]

Kong L, Wang X, Choe DW, Polley M, Burnett BG, Bosch-Marcé M, Griffin JW, Rich MM, Sumner CJ. Impaired synaptic vesicle release and immaturity of neuromuscular junctions in spinal muscular atrophy mice. J Neurosci. 2009; 29:842–51. [PubMed: 19158308]

Lichtman JW, Sanes JR. Watching the neuromuscular junction. J Neurocytol. 2003; 32:767–75. [PubMed: 15034266]

Ling KK, Gibbs RM, Feng Z, Ko CP. Severe neuromuscular denervation of clinically relevant muscles in a mouse model of spinal muscular atrophy. Hum Mol Genet. 2012; 21:185–95. [PubMed: 21968514]

Lu J, Tapia JC, White OL, Lichtman JW. The interscutularis muscle connectome. PLoS Biol. 2009; 7:e32. [PubMed: 19209956]

Marques MJ, Conchello JA, Lichtman JW. From plaque to pretzel: fold formation and acetylcholine receptor loss at the developing neuromuscular junction. J Neurosci. 2000; 20:3663–75. [PubMed: 10804208]

Martínez-Hernández R, Bernal S, Also-Rallo E, Alías L, Barceló M, Hereu M, Esquerda JE, Tizzano EF. Synaptic defects in type I spinal muscular atrophy in human development. J Pathol. 2012

McArdle JJ, Angaut-Petit D, Mallart A, Bournaud R, Faille L, Brigant JL. Advantages of the triangularis sterni muscle of the mouse for investigations of synaptic phenomena. J Neurosci Methods. 1981; 4:109–15. [PubMed: 7278363]

Misgeld T, Burgess RW, Lewis RM, Cunningham JM, Lichtman JW, Sanes JR. Roles of neurotransmitter in synapse formation: development of neuromuscular junctions lacking choline acetyltransferase. Neuron. 2002; 36:635–48. [PubMed: 12441053]

Murray L, Gillingwater TH, Kothary R. Dissection of the *Transversus Abdominis* muscle for whole-mount neuromuscular junction analysis. J Vis Exp. 2014 in press.

Murray LM, Beauvais A, Bhanot K, Kothary R. Defects in neuromuscular junction remodelling in the $Smn^{2B/-}$ mouse model of spinal muscular atrophy. Neurobiol Dis. 2012; 49C:57–67. [PubMed: 22960106]

Murray LM, Comley LH, Thomson D, Parkinson N, Talbot K, Gillingwater TH. Selective vulnerability of motor neurons and dissociation of pre- and post-synaptic pathology at the neuromuscular junction in mouse models of spinal muscular atrophy. Hum Mol Genet. 2008a; 17:949–62. [PubMed: 18065780]

Murray LM, Gillingwater TH, Parson SH. Using mouse cranial muscles to investigate neuromuscular pathology *in vivo*. Neuromuscul Disord. 2010a; 20:740–3. [PubMed: 20637618]

Murray LM, Lee S, Baumer D, Parson SH, Talbot K, Gillingwater TH. Pre-symptomatic development of lower motor neuron connectivity in a mouse model of severe spinal muscular atrophy. Hum Mol Genet. 2010b; 19:420–33. [PubMed: 19884170]

Murray LM, Talbot K, Gillingwater TH. Neuromuscular synaptic vulnerability in motor neurone disease: amyotrophic lateral sclerosis and spinal muscular atrophy. Neuropathol Appl Neurobiol. 2010c; 36:133–56. [PubMed: 20202121]

Murray LM, Thomson D, Conklin A, Wishart TM, Gillingwater TH. Loss of translation elongation factor (*eEF1A2*) expression *in vivo* differentiates between Wallerian degeneration and dying-back neuronal pathology. J Anat. 2008b; 213:633–45. [PubMed: 19094180]

Sanes JR, Lichtman JW. Development of the vertebrate neuromuscular junction. Annu Rev Neurosci. 1999; 22:389–442. [PubMed: 10202544]

Sanes JR, Lichtman JW. Induction, assembly, maturation and maintenance of a postsynaptic apparatus. Nat Rev Neurosci. 2001; 2:791–805. [PubMed: 11715056]

Santos AF, Caroni P. Assembly, plasticity and selective vulnerability to disease of mouse neuromuscular junctions. J Neurocytol. 2003; 32:849–62. [PubMed: 15034272]

Seburn KL, Nangle LA, Cox GA, Schimmel P, Burgess RW. An active dominant mutation of glycyl-tRNA synthetase causes neuropathy in a Charcot-Marie-Tooth 2D mouse model. Neuron. 2006; 51:715–26. [PubMed: 16982418]

Sleigh JN, Gillingwater TH, Talbot K. The contribution of mouse models to understanding the pathogenesis of spinal muscular atrophy. Dis Model Mech. 2011; 4:457–67. [PubMed: 21708901]

Sleigh JN, Grice SJ, Burgess RW, Talbot K, Cader MZ. Neuromuscular junction maturation defects precede impaired lower motor neuron connectivity in Charcot-Marie-Tooth type 2D mice. Hum Mol Genet. 2014 in press.

Spillane J, Beeson DJ, Kullmann DM. Myasthenia and related disorders of the neuromuscular junction. J Neurol Neurosurg Psychiatry. 2010; 81:850–7. [PubMed: 20547629]

Stum M, McLaughlin HM, Kleinbrink EL, Miers KE, Ackerman SL, Seburn KL, Antonellis A, Burgess RW. An assessment of mechanisms underlying peripheral axonal degeneration caused by aminoacyl-tRNA synthetase mutations. Mol Cell Neurosci. 2010; 46:432–43. [PubMed: 21115117]

Thomson SR, Nahon JE, Mutsaers CA, Thomson D, Hamilton G, Parson SH, Gillingwater TH. Morphological characteristics of motor neurons do not determine their relative susceptibility to

degeneration in a mouse model of severe spinal muscular atrophy. PLoS One. 2012; 7:e52605. [PubMed: 23285108]

Torres-Benito L, Neher MF, Cano R, Ruiz R, Tabares L. SMN requirement for synaptic vesicle, active zone and microtubule postnatal organization in motor nerve terminals. PLoS One. 2011; 6:e26164. [PubMed: 22022549]

Tsujihata M, Hazama R, Yoshimura T, Satoh A, Mori M, Nagataki S. The motor end-plate fine structure and ultrastructural localization of acetylcholine receptors in amyotrophic lateral sclerosis. Muscle Nerve. 1984; 7:243–9. [PubMed: 6708970]

Turner BJ, Talbot K. Transgenics, toxicity and therapeutics in rodent models of mutant SOD1-mediated familial ALS. Prog Neurobiol. 2008; 85:94–134. [PubMed: 18282652]

Valdez G, Tapia JC, Kang H, Clemenson GD Jr, Gage FH, Lichtman JW, Sanes JR. Attenuation of age-related changes in mouse neuromuscular synapses by caloric restriction and exercise. Proc Natl Acad Sci U S A. 2010; 107:14863–8. [PubMed: 20679195]

Walsh MK, Lichtman JW. *In vivo* time-lapse imaging of synaptic takeover associated with naturally occurring synapse elimination. Neuron. 2003; 37:67–73. [PubMed: 12526773]

Wokke JH, Jennekens FG, van den Oord CJ, Veldman H, Smit LM, Leppink GJ. Morphological changes in the human end plate with age. J Neurol Sci. 1990; 95:291–310. [PubMed: 2358822]

Wu H, Mei L. Morphological analysis of neuromuscular junctions by immunofluorescent staining of whole-mount mouse diaphragms. Methods Mol Biol. 2013; 1018:277–85. [PubMed: 23681637]

Highlights

- Mouse hind-limb lumbrical muscles can be easily dissected and whole-mounted.
- The entire lumbrical innervation pattern can be viewed without sectioning.
- Developmental and degenerative NMJ phenotypes can be accurately scored.
- NMJ phenotypes pertinent to neuromuscular pathology can be readily characterised.

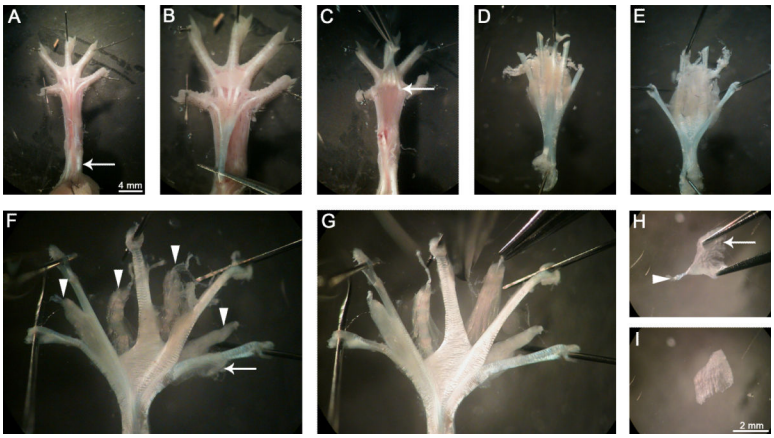

Figure 1. Hind-limb lumbrical muscles can be easily dissected

Immediately after culling, the hind-limbs are removed and overlying skin detached. The leg (left in this figure) is then pinned out ventral side up (A), and the remaining plantar skin dissected away revealing the tendons in the foot. The overlying FDB tendon is cut transversely close to the ankle, lifted up towards the digits, and removed completely by cutting the distal ends of the tendon at the level of the metatarsophalangeal joints (A, arrow). The underlying FDL tendon, from which the lumbricals originate, is now visible (B). This tendon is also cut proximally and pulled back towards the digits (C). The tendons, along with connective tissue and the distal ends of the lumbricals, are cut close to the base of the digits (C, arrow) and the plantar muscle mass lifted out. The FDL tendon is then spread and tautly pinned ventral side up (E, not D). The connective tissue is carefully cleared, revealing the underlying lumbricals (arrowheads) between the tendon ends (from medial to lateral, the first to fourth) (F). The FDL muscles (F, arrow) can be detached to increase visibility of the lumbricals (G). Excess connective tissue is removed by blunt dissection in the regions between the lumbricals and the tendons, before fixation. Lumbrical muscles are excised and further connective tissue (H, arrow) removed. Once cleaned up, the distal FDB tendon (arrowhead) is disconnected, and the muscle is ready for staining (I). Lumbrical muscles were dissected from a two month-old wild-type mouse in this figure.

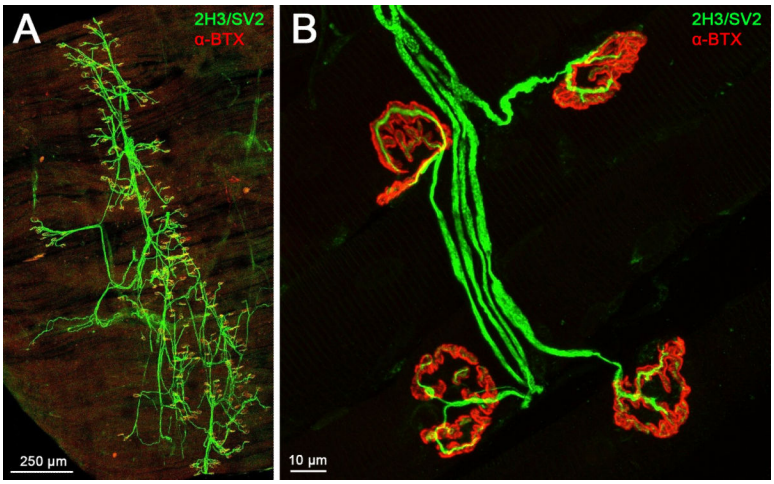

Figure 2. The entire innervation pattern of lumbrical muscles can be imaged and NMJs examined

A. A representative confocal micrograph of a wild-type mouse hind-limb lumbrical muscle at post-natal day 15. The entire innervation pattern is visible in the thin, whole-mount preparation, obviating the need for muscle sectioning. Two separate “collapsed” images were tiled together to produce this figure. **B.** NMJs can be viewed in fine detail, allowing accurate characterisation of a number of phenotypes (see Fig. 3). This image shows example NMJs from a two month-old wild-type mouse. For this and the subsequent figure, nervous tissue is stained green (2H3, neurofilament, and SV2, synaptic vesicle 2) and post-synaptic AChRs are stained red (-BTX, -bungarotoxin). 10× and 63× objectives were used to produce the images in panels A and B, respectively.

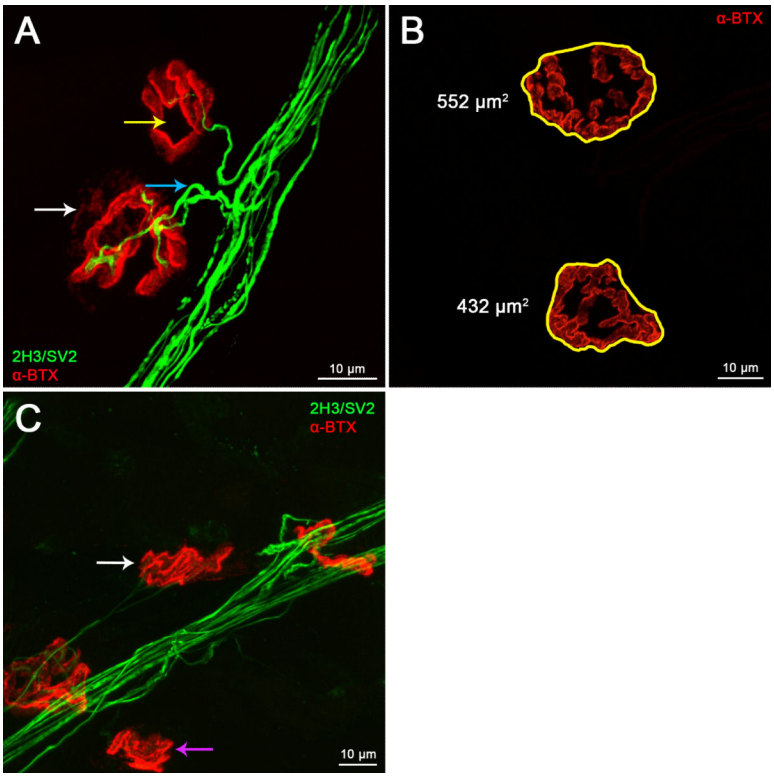

Figure 3. Lumbrical NMJs can be accurately assayed for developmental and denervation phenotypes

A. In early post-natal development, NMJs undergo a number of maturational processes that can be assessed using confocal microscopy. Synapse elimination can be scored by calculating the percentage of NMJs that remain polyinnervated (A, blue arrow), and the plaque-to-pretzel transition can be measured up to one month post-birth by counting the number of perforations per post-synaptic endplate (A, yellow arrow). These maturational processes occur during the first few post-natal weeks in wild-type animals, and can be studied in neurological disease models to determine defective neuromuscular development. **B–C.** Synaptic growth and neurodegeneration can also be evaluated in wild-type and disease model mice. Confocal Z-stack images can be used to measure post-synaptic area and average fluorescence intensity (B), while loss of lower motor neuron connectivity can be determined by scoring the percentage of NMJs displaying a lack of overlap in pre-and post-synaptic staining (C). The white arrow in panel A identifies a partially denervated synapse, while the purple and white arrows in panel C highlight fully and partially denervated NMJs, respectively. Panels A and C show NMJs from a two month-old mouse model of the peripheral neuropathy Charcot-Marie-Tooth disease type 2D (*Gars*$^{Nmf249/+}$), and panel B depicts two month-old wild-type endplates. A 63x objective was used to produce the images for this figure.